View metadata, citation and similar papers at core.ac.uk

brought to you by CORE

provided by Missouri University of Science and Technology (Missouri S&T): Scholars' Mine

Missouri University of Science and Technology

Scholars' Mine

International Specialty Conference on Cold-Formed Steel Structures

(1992) - 11th International Specialty Conference on Cold-Formed Steel Structures

Oct 20th, 12:00 AM

Tests of Profiled Steel Decks with V-stiffeners

E. S. Bernard

Russell Q. Bridge

Gregory J. Hancock

Follow this and additional works at: https://scholarsmine.mst.edu/isccss

 Part of the Structural Engineering Commons

Recommended Citation

Bernard, E. S.; Bridge, Russell Q.; and Hancock, Gregory J., "Tests of Profiled Steel Decks with V-stiffeners" (1992). *International Specialty Conference on Cold-Formed Steel Structures*. 1.
https://scholarsmine.mst.edu/isccss/11iccfss/11iccfss-session1/1

This Article - Conference proceedings is brought to you for free and open access by Scholars' Mine. It has been accepted for inclusion in International Specialty Conference on Cold-Formed Steel Structures by an authorized administrator of Scholars' Mine. This work is protected by U. S. Copyright Law. Unauthorized use including reproduction for redistribution requires the permission of the copyright holder. For more information, please contact scholarsmine@mst.edu.

Eleventh International Specialty Conference on Cold-Formed Steel Structures
St. Louis, Missouri, U.S.A., October 20-21, 1992

TESTS OF PROFILED STEEL DECKS WITH V-STIFFENERS

E. S. Bernard R. Q. Bridge G. J. Hancock

Centre for Advanced Structural Engineering
School of Civil and Mining Engineering
University of Sydney

SYNOPSIS

The size and position of intermediate stiffeners in the compression flanges of thin-walled profiled steel decks exerts a strong influence on the dominant buckling mode of the flange. The ability of the deck to provide both high load carrying capacity before the onset of elastic buckling and a high ultimate load capacity may therefore be affected.

A programme of tests to determine the effectiveness of intermediate stiffeners in controlling buckling modes has been undertaken. A series of specimens were loaded in pure bending resulting in various buckling waveforms prior to ultimate failure through a plastic collapse mechanism. All specimens were brake-pressed to designs that were chosen to ensure that the primary buckling took place in the elastic range and was not affected by plasticity.

The experimentally determined buckling stresses were found to be comparable with studies performed using a computer analysis based on the finite strip method in which both local and distortional buckling modes were predicted. The test rig developed for the programme successfully approximated the boundary conditions implicit in the numerical model and prevented premature failure due to localised stressing at the specimen ends.

A simplified design procedure for distortional buckling is proposed. The existing design procedure for local buckling in the Australian Standard AS1538-1988 is confirmed.

1 INTRODUCTION

The size and position of intermediate stiffeners in the compression flanges of thin-walled profiled steel decks exerts a strong influence on the dominant buckling mode of the flange. Apart from the local mode of buckling involving deformation of the flat plate regions between stiffeners or webs, flanges may display distortional modes where the stiffener moves normal to the plane of the element being stiffened. This mode involves deformation of the stiffener in such a manner that membrane stresses in the stiffener and the adjacent plate become involved in the solution of the governing equations (Hancock, 1985; Lau and Hancock, 1988). Other researchers have described this mode by a variety of names including local-torsional (Sridharan, 1982).

Test sections composed of high strength steel were brake-pressed with a variety of 'V' shaped intermediate stiffeners in the compression flanges forming a progression from small to large stiffeners. These were intended to span a range that would encompass both local and distortional modes of buckling. The test rig employed applied pure bending and successfully maintained the specimen boundary conditions so as to prevent localised stressing.

The purpose of this paper is the description of the experiments and the presentation of the results of the current test programme, as well as comparisons with numerical analyses based on the finite strip method of elastic buckling analysis (Cheung, 1976). A simplified design procedure for distortional buckling is proposed. The existing design procedure for local buckling in the Australian Standard AS1538-1988 is confirmed.

2 TEST SECTIONS

2.1 Geometry

The present deck profiles were selected to exhibit a variety of buckling modes ranging from local to distortional. The buckling behaviour was expected to progress from distortional for small intermediate stiffeners to local for large stiffeners. Several specimens would exhibit both modes of buckling, one occurring at a moment greater than the other. These were expected to show an 'interaction' of buckling waveforms. The exact nature of this behaviour was of considerable interest in this investigation. These expectations were based on the analyses described in Section 2.2.

As depicted in Fig. 1, the intermediate stiffeners were in the shape of a 'V' with an enclosed angle of 90° at the base. This shape was selected because it was simple to produce and presented few parameters for variation. As the height s (or depth) of the stiffener increased from 2 to 10 mm (0.0787 to 0.3937 inch), the proportions of the 'V' remained the same. The intermediate stiffeners were in the middle of the compression flanges. The full sections consisted of a trapezoidal shape repeated as four longitudinal ribs. Total width of the folded sections was approximately 785 mm (30.9 inch) while the length was 2000 mm (78.7 inch).

Labelling of specimens consisted of a prefix IST (Intermediate Stiffener Test) followed by a numeral '4' and the height of the stiffener in millimetres. As most specimens had a duplicate, there was an additional suffix of either A or B. Hence

specimen IST47B refers to the second specimen with a 7 mm (0.2756 inch) stiffener. Apart from the twelve specimens with intermediate stiffeners, there were six specimens without stiffeners used as zero-height controls and as simple geometries for numerical comparison. These had the designation ST21, ST22 and ST23. Listings of the fold coordinates of the cross-sections at both ends of each specimen are contained in the report by Bernard, Bridge and Hancock (1992).

2.2 Theoretical Estimates

A finite strip elastic buckling analysis developed by Hancock (1977) was incorporated into a program called EDB and used to estimate the elastic critical stress at which each specimen would buckle. The analysis is based on the method published by Cheung (1976) which sub-divided a prismatic section into longitudinal strips, each of which buckled with a displacement profile described by a trigonometric function in the longitudinal direction and a simple polynomial function in the transverse direction. By applying a stress distribution consistent with flexural loading (in this case based on simple engineering bending theory) and analysing for a variety of buckling half-wavelengths, the elastic critical buckling stress was established through selection of the minimum resultant load factor.

The geometry of each specimen was measured and a mean and standard deviation determined for the primary geometric parameters such as stiffener height, flange width and overall section depth. The elastic critical buckling stress for both local and distortional modes of buckling were determined, firstly for the mean geometry, then the mean plus/minus one standard deviation. The nominal dimensions were also used in a comparative analysis. These analyses were used to produce the numerical results shown in Figs. 4 to 6. The sections were bent about their minor axis, thus an overall mode of buckling did not exist.

Due to the symmetry existent in each section, only one half of one rib (out of four in each deck, only ST23 having 3 ribs) was analysed allowing a great saving in the number of strips used. The various buckling modes encountered in this series of tests are shown in Fig. 2. The only mode of buckling encountered that was not symmetric was an anti-symmetric local mode involving the two flat elements on either side of each intermediate stiffener. This was found to involve torsional deformation of the intermediate stiffener in those specimens with small stiffeners, but not for those with larger stiffeners. However, as it displayed a critical stress that was almost the same as the symmetric local mode, the two modes have been considered essentially identical as far as the load factor is concerned.

3 MECHANICAL PROPERTIES

3.1 General

The test specimens examined in this investigation were folded to shape using a Cincinnati Milacron 3.6 m (142 inch) manually operated brake press. The strip used was cold-reduced aluminium/zinc (Zincalume) coated Grade G550–AZ150 steel supplied by BHP Sheet and Coil Products, Port Kembla. The designation AZ150 refers to its coating of 150 g/m^2 of aluminium and zinc. The composition

of the coating was confirmed by the first author to be 33% Al, 67% Zn using x-ray diffraction techniques. The strip had a minimum yield strength of 550 MPa (79.8 ksi), a total coated thickness of approximately 0.63mm (0.0248 inch) and conformed to AS1397 (SAA 1984) standards for rolled strip.

3.2 Coupon Tests

The conclusion of Kwon and Hancock (1991), that mechanical property variation within brake-pressed sections was negligable and of little consequence to structural performance, was assumed to hold true for the current specimens since both were similarly manufactured. Tensile coupon tests were therefore performed using only the strip at the centre of the sections' flat elements.

The tensile tests indicated that for the flat-plate regions, the elastic modulus based on the full coated thickness was 220 GPa (31908 ksi), while for the base metal alone (the Zincalume having been etched off) a higher modulus of 230 GPa (33359 ksi) was measured. The mean 0.2% yield stress of 653 MPa (94.7 ksi, uncoated base metal) was higher than the minimum specified and was essentially the same as the mean ultimate tensile strength of 656 MPa (95.1 ksi). This compared favourably with AS1397-1984 which states that yield stress and ultimate strength are the same for grade G550 steel of less than 1.0 mm (0.03937 inch) thickness.

3.3 Effective Thickness

The specified nominal thickness of the sheet was 0.60 mm (0.026 inch). Type AZ150 coating is specified in AS1397–1984 as being equivalent to 0.05 mm of Aluminium Zinc coating.

An independent determination of the thickness of the base metal and coating was made. The technique involved the use of a Philips 505 Scanning Electron Microscope and a micrometer. The results indicate a mean base metal thickness of 585μm (0.585 mm, 0.02303 inch) with Zincalume coating thicknesses of 20μm and 25μm on respective strip surfaces (totalling 0.045 mm). The surfaces of the coatings were quite rough while the base metal exhibited less thickness variation. Nevertheless, base metal thickness varied from 580 to 588 μm. This compared favourably with micrometer measurements of 0.590 mm most probably due to the fact that the micrometer was likely to measure only the thickest part of the sheet at the position of the micrometer.

3.4 Residual Stresses

Longitudinal residual stresses may be present in a section as a result of manufacture. These stresses are able to exert a considerable influence on buckling loads because they modify the apparent elastic critical buckling stress of a section. In brake-pressed decks, the shape of the profile is produced by applying transverse bending forces to create longitudinal folds, hence longitudinal residual stresses are generally small unless they originate from some process prior to folding (such as the rolling of the strip).

To investigate the presence and severity of residual stress, several representative decks were selected for testing. IST412 and IST410 were chosen because they had

the largest stiffener and, it was assumed, would therefore have the largest residual stress in the neighbourhood of their stiffeners.

In general, the nett longitudinal residual stress was found to be small, of the order of 5-10 MPa (0.72-1.45 ksi). Residual flexural stress was much greater at 80-120 MPa (11.6-17.4 ksi). Furthermore, the 'polarity' of the flexural stress was related to whether the deck was folded with the concave surface of the strip facing up or down (as it came off the coil). In order to know the distribution of this stress in the rest of the specimens, knowledge of the sense of the concavity of the feedstock before folding was required. Unfortunately such records were not kept by the brake-presser.

The distribution of nett longitudinal residual stress did not reveal a consistent pattern from the small number of specimens tested in this programme. Since the stresses were more than an order of magnitude less than the mean critical elastic buckling stress of each specimen they were considered to be of little consequence.

4 PREPARATION FOR TESTING

4.1 Boundary Conditions

Numerical analyses of the tested geometries involved specific boundary conditions. These conditions resulted from the limitations of the finite strip buckling method (Section 2.2) and had to be adhered to, or at least approximated, in the test procedure in order to allow accurate comparisons of the theory with tests.

The theoretical end conditions assumed that a rigid membrane existed in a transverse plane through the end section, preventing section distortion. However, the ends were free to warp longitudinally in the distortional buckling mode where membrane bending of the stiffeners occurred. The longitudinal free edges of the model were in tension and therefore did not undergo buckling. The phenomenon of flange curling, which was believed to have occurred in the experiments, was not modelled. The numerical model assumed pure and uniform flexure.

In order to approximate the boundary conditions required by the numerical models and to eliminate local stressing of the sections, uniform flexural stress was required to be imposed through rigid end plates without point loads contacting the specimen. To determine the most suitable physical means of achieving rigidity and moment transfer through end plates, a brief investigation of two proposals for end fixity was carried out. These became known as the Cantilever Tests as they were performed on one metre long offcuts tested in cantilever action.

4.2 Cantilever Tests

Two proposals for ensuring the maintenance of the required end boundary conditions were investigated. The first involved clamping the ends of the profiles between steel blocks which had been machined to match the geometry of the section being tested. The second proposal involved casting the section ends into Patternstone, with subsequent application of a very high compressive stress to ensure that there was sufficient friction established to prevent pull-out of the specimen under flexural actions.

The results of these tests demonstrated the superiority of the Patternstone castings in providing end fixity. This method was used in all subsequent tests, except that all steel surfaces were galvanised, thus decreasing the friction between the patternstone and the surfaces of the rig. While it is known that the coefficient of friction on zinc surfaces is less than that for steel, adverse effects were not encountered in the tests.

This method was highly successful in approximating the rigid end plate and thus preventing section distortion and localised stressing. However, it violated the theoretical requirement of permitting longitudinal warping and thus was presumed to have had an adverse effect on the distortional mode of buckling (the severity of which was unknown but likely to be small for the present test series).

4.3 Test Rig Design

The design of the test rig was based on a variety of considerations. The primary requirement was for a test apparatus that would satisfactorily impose the requisite uniform and pure flexural stress in the specimen whilst maintaining the boundary conditions implied in the comparative numerical models. It also had to remain inexpensive and simple to operate. A schematic diagram of the subsequent rig design is shown in Fig. 3. This indicates the major dimensions and important components of the apparatus.

An important consideration in the design of the rig was that the specimen was expected to behave in a brittle manner upon ultimate failure as spatial plastic mechanisms formed in the sections (Key, Hasan and Hancock,1988; Rasmussen and Hancock,1991). A common course of action to overcome such stability problems in the unloading portion of a load-response curve is to employ servo-controlled hydraulic actuators to impose load where the actuators are controlled by a displacement of the test specimen which monotonically increases with load. Due to the difficulty of using such equipment for decking sections (where two loading devices are required) a cheaper alternative was pursued – that of manually operated screw jacks. The main operational disadvantage caused by this choice was the difficulty in maintaining uniform load distribution in both ends of the specimen.

The magnitude of the point loads imposed on the specimen were small, of the order of 10 kN (2250 lb). Loadcells capable of good accuracy in this low load range were not available commercially, hence suitable equipment was designed and manufactured. A reliable design was arrived at by the first author with a compressive load range of 0.0 to 6.0 kN (1350 lb) and a sensitivity of 1 part in 500.

5 FLEXURAL TESTS

5.1 Execution of Tests

Eighteen specimens were tested using the above mentioned rig in the manner described below. Each test involved the application of point loads at four locations, two adjacent to each end of the specimen as indicated in Fig. 3. Moment was thereby imparted into the specimen through the rigid Patternstone connections between the deck and moment transfer frames. As the displacement of the screw

jacks was increased, the loads and associated moment also increased, resulting in flexure of the specimen. Displacements were applied equally at both ends of the specimen so as to induce a uniform moment. As each increment was applied, measurements of load, strains and displacements were made. If a discrepancy in load between the two ends of the specimen (known as the North and South ends) occurred, a correction was made in the next increment so as to maintain uniformity longitudinally. Equality of load between each of the jacks in the transverse direction was not as important because the large stiffness of the moment transfer frames ensured that torsion did not occur in the specimen. In this way, load could be applied in approximately equal increments up to ultimate failure in such a manner as to maintain uniform moment while retaining the benefits of displacement controlled loading.

Prior to testing, installation of the specimen in the test rig was performed. Installation required that all High Strength Friction Grip (HSFG) bolts used to apply end clamping stress be tensioned to their full strength with the patternstone blocks correctly positioned relative to the moment transfer frames. The most important requirement was for the specimen to be aligned parallel with the moment transfer frames and perpendicular to the pivot axes of the support rollers; failure to do so could result in non-uniform bending of the specimen. After tensioning, 16 to 18 displacement transducers (200 mm, 7.87 inch extension) were secured to the underside of the specimen. Displacement dial gauges (0.0025 mm, 0.00001 inch accuracy) were used to measure slip of the patternstone blocks relative to their anchorage.

Immediately prior to testing, a levelling survey along the length of the specimen was undertaken with a Wild NA2 automatic level and target. The effective accuracy of this method for determining the initial curvature of the specimen was ± 0.1 mm per reading. The presence of an initial curvature in the specimen was due to the difficulty of achieving exactly zero moment prior to engaging the screw jacks and applying external load. The 'pre-load' moment was deduced by multiplying the initial curvature of the specimen by its stiffness at the start of loading. This method was satisfactory for most specimens but was subject to errors in both curvature and stiffness determination. The pre-load moment was initially assumed to be negligible and several specimens were tested before its true magnitude was appreciated. Initial curvature measurements were therefore not taken for some of the early tests and estimates of pre-load moment were made by averaging results for the other specimens. Once pre-load was established, it was added to the test readings to arrive at the true state of stress existing at any point in the specimen's load history.

A cycle of low load magnitude was imposed at the start of loading. This was found to improve the 'smoothness' of the tangent stiffness graphs because it allowed the two screw jack operators to find a balance between the load they each applied and hence maintain a more uniform moment distribution. Most of the specimens displayed a moment-curvature response that featured some degree of unevenness in both the linear-elastic and post-buckled regions. This was a result of the use of redundant displacement controlled screw jacks. The evenness of the response improved as the operators gained experience.

When the specimen was well within the post-buckled range measurements of buckled wavelengths and notes on waveform structure were taken. As the load

approached the advanced plastic region the displacement increment magnitude was increased to maintain approximately equal load increment size. Upon failure of the specimen the load was removed and final measurements made.

Vertical displacements at up to 13 points were recorded at 150 mm (5.9 inch) centres along the length of each specimen by means of Linear Voltage Displacement Transducers (LVDT's). Length-wise profiles of these displacement readings were adjusted by means of a least squares approximation to either a parabolic or circular segment. The algebraic expression for this adjustment was then differentiated twice to yield a curvature estimate at each load level, and differentiated once more with respect to moment to estimate tangent stiffness. It is commonly encountered in experimental measurements that differentiation of data may produce highly variable results. The curvature graphs were therefore 'smoothed' through the application of 4 and 8 point polynomial least squares approximations leading to the stiffness estimates described in the following section.

5.2 Test Results

The buckling and ultimate load results for all specimens are summarized in Tables 1 and 2. The buckling half-wavelength comparisons for all specimens are contained in Table 3. Complete moment-curvature and stiffness graphs are contained in the report by Bernard, Bridge and Hancock (1992). Strain measurements for those specimens with resistance strain gauges attached are also included together with variance data on transducer readings.

In general, the results showed a well defined point of elastic buckling for most specimens. Post-buckled performance varied between straight line behaviour with a discernable post-buckled stiffness, to well rounded behaviour of monotonically decreasing stiffness. All tests culminated in a brittle failure involving a spatial plastic mechanism (Murray and Khoo, 1981) centred on either a locally or distortionally buckled cell. The point(s) of ultimate failure along the length of each specimen varied considerably (even between ribs on the same specimen) indicating that uniform moment was maintained throughout the load history of each test. Unloading curves were not obtained for any of the specimens due to the instability associated with brittle failure resulting from the spatial plastic mechanisms in the test pieces.

The magnitude of the moment to cause elastic buckling showed a consistent rise with increasing stiffener size (Tables 1 and 2, Figs. 4 and 5). The results demonstrated variability in elastic buckling stress for specimens of similar stiffener size. However this was within experimental limits.

The elastic critical buckling moment for both local and distortional modes was determined by a variety of methods allowing for the range in quality and behaviour of the decks tested. Method 1 was based on the point of inflexion in the falling tangent stiffness curve immediately after the commencement of softening (Davids and Hancock, 1986) and has been called the Stiffness Method. Method 2 was the well known technique based on the intersection of tangents to the pre- and post-buckled straight line portions of the moment-curvature graph for each specimen. Method 3 was applicable to those specimens with resistance strain gauges attached and was described by Venkataramaiah and Roorda (1982) as the Strain Reversal method. The same authors referred to the Vertical Tangent method (Coan, 1951)

as being superior to the Strain Reversal method, however this method was not used as several sets of strain readings proved unsuitable. The 'deflection squared' (or $P - w^2$) method, also by Venkataramaiah and Roorda (1982), was attempted but proved to be unsuitable for deflection measurements obtained in this test programme.

Ultimate moments (Table 1, Fig. 8) were found to increase with stiffener size for the larger depths. A low level of variability was found for specimens of similar stiffener size. The tangent stiffness was found to be subject to considerable variation, even in the linear-elastic region. The post-buckled tangent stiffness appeared to depend on the mode of buckling – local buckling resulting in a substantially greater reduction in stiffness than distortional buckling.

The buckled waveforms, both local and particularly distortional, were observed to move along the specimens during the tests. Individual distortional buckles appeared to form quite independently of each other, progressively moving closer together as loading advanced and more waveforms 'popped' into the flanges. The sudden changes in waveform number were often violent and accompanied by very loud 'bangs'. Interaction between the local and distortional modes did not occur in a consistent manner. When the distortional mode occurred before the local, the smaller local waveforms were not superimposed on the larger distortional ones, but instead formed between the longer wavelength distortional buckles. They did so in groups of two to four depending on how far apart the larger waveforms originally were and consequently did not have a consistent wavelength. When the distortional mode occurred after the local, the shorter waveforms were superimposed on the distortional buckles which formed 'under' them.

6 COMPARISON OF BUCKLING STRESS WITH THEORY

The experimental buckling stresses for both local and distortional modes of failure were compared with estimates determined using the finite strip buckling analysis program (EDB) described in Section 2.2. The experimental results are shown in Tables 1 (local buckling) and 2 (distortional buckling) and data has been presented graphically in Figs. 4 to 6.

A separation of results between the local and distortional buckling modes has been made for the purpose of clarity. Both these modes were evident in several specimens (usually occurring at different moments), while in others only one mode was evident throughout the loading history. Each occurrence of buckling has been recorded as a separate point in Figs. 4 to 6.

In the case of local buckling, there was good agreement between experimental and theoretical results (Fig. 4 (d)). The individual test results fell within the envelope for one standard deviation variability in the geometry (see Section 2.2 and Fig. 4(c)) and showed a steady increase in elastic buckling stress with stiffener size.

For the distortional mode, the test results showed very good agreement with the theoretical estimates that incorporated the compression flange depression measured in most of the specimens (Fig. 5(d)). However, there was a noteable difference when the numerical model did not incorporate the flange depression

(Fig. 5(c)), particularly for those specimens with small ($\leq$4.0 mm, 0.157 inch) intermediate stiffeners. In both Figs. 5(c) and (d) the straight line is the line of best fit to the experimentally determined points indicated in Fig. 5(b). This demonstrates the important influence that the compression flange depression in the vicinity of the intermediate stiffener has on the critical buckling stress for the distortional mode.

The experimental values of elastic critical buckling stress for those specimens without intermediate stiffeners (ST21, ST22, ST23) were found to compare well with theoretical estimates (Fig. 6(a)-(d), Table 1). The buckling half-wavelengths (Table 3) also showed good agreement, although not for all specimens. Compression flange depressions did not occur in any of this set of specimens due to a lack of intermediate stiffener.

The numerical results for the ideal geometries, that is, with dimensions as specified to the manufacturer, are shown in Fig. 7. They were found to fit within the variability envelopes based on the actual geometries for both the local and distortional modes, except for small stiffeners. This again indicates the influence of the compression flange depression on the elastic critical buckling stress for the distortional mode.

Ultimate moments at failure (Fig. 8) showed a consistent rise with increased stiffener size. In fact, the increase was enough to warrant attention as an economical means of increasing capacity since the price was only a minor increase in the amount of strip used in the stiffeners.

7 COMPARISON WITH DESIGN METHODS

7.1 Distortional Buckling

The Winter Formula is commonly used in design procedures to determine an estimate of the ultimate load carrying capacity of plates in compression (eg. AISI-1989; AS1538-1988). In its usual form it is expressed

$$\frac{b_e}{b} = \sqrt{\frac{\sigma_{le}}{F_y}}\left(1 - 0.22\sqrt{\frac{\sigma_{le}}{F_y}}\right) \tag{1}$$

where b_e is the effective part of the plate width b, σ_{le} is the elastic buckling stress and F_y is the yield stress.

Kwon and Hancock (1991) proposed a modification of this formula to permit application to the distortional mode of buckling for columns undergoing essentially uniform compression. This was done in two stages. At first, the elastic local buckling stress (σ_{le}) was replaced by the elastic distortional buckling stress (σ_{de}) to arrive at

$$\frac{b_e}{b} = 1 \qquad \lambda \leq 0.673 \tag{2a}$$

$$\frac{b_e}{b} = \sqrt{\frac{\sigma_{de}}{F_y}}\left[1 - 0.22\sqrt{\frac{\sigma_{de}}{F_y}}\right] \qquad \lambda \geq 0.673 \tag{2b}$$

where

$$\lambda = \sqrt{\frac{F_y}{\sigma_{de}}} \tag{2c}$$

In this form, it was assumed that all plate elements forming the cross-section were reduced to effective widths in the same proportions. This was equivalent to

$$\frac{A_e}{A} = \sqrt{\frac{\sigma_{de}}{F_y}}\left(1 - 0.22\sqrt{\frac{\sigma_{de}}{F_y}}\right) = \frac{\sigma_u}{F_y} \tag{3}$$

where A_e is the effective part of the gross section area A and σ_u is the stress at ultimate load based on the gross area A.

Kwon and Hancock found that this approach yielded unconservative estimates under certain circumstances and thus produced their 'Design Proposal 2' in which the exponent of the (σ_{de}/F_y) term in Equation (2b) was changed from 0.5 to 0.6 and the 0.22 coefficient increased to 0.25, thus

$$\frac{b_e}{b} = 1 \qquad \lambda \leq 0.561 \tag{4a}$$

$$\frac{b_e}{b} = \left(\frac{\sigma_{de}}{F_y}\right)^{0.6}\left(1 - 0.25\left(\frac{\sigma_{de}}{F_y}\right)^{0.6}\right) \qquad \lambda \geq 0.561 \tag{4b}$$

where

$$\lambda = \sqrt{\frac{F_y}{\sigma_{de}}} \tag{4c}$$

As for equation (2), this reduction of the effective widths was performed for all the elements of the section and thus the reduction was equivalent to reducing the gross area to an effective area.

If a similar approach is applied to members in flexure, then, by direct analogy with Equation (3), the effective section modulus (Z_e) is calculated as

$$\frac{Z_e}{Z} = \sqrt{\frac{\sigma_{de}}{F_y}}\left(1 - 0.22\sqrt{\frac{\sigma_{de}}{F_y}}\right) = \frac{\sigma_u}{F_y} \tag{5}$$

leading to the ultimate moment capacity

$$M_u = F_y Z_e = \sigma_u Z \tag{6}$$

where Z is the section modulus of the gross section.

In the present test programme, the nondimensionalised ultimate stress results (σ_u/F_y) for those specimens that displayed distortional buckling prior to failure have been plotted in Fig. 9. These points indicate good agreement with the Winter Formula provided that the effective section modulus of each specimen is determined according to the formula and not the effective widths of individual elements. The additional points are those resulting from the earlier work by Lau and Hancock (1988) and Kwon and Hancock (1991). Note that there is no apparent difference between specimens that experienced local buckling before distortional, distortional before local, or only distortional buckling, provided that distortional buckling occurred at some point in the loading history.

Table 4 presents the experimental data from which Fig. 9 is derived. Note that σ_{de} has been derived by numerical means based on the measured geometry of each specimen. This was shown in Fig. 5(d) to be a very good estimate of the experimental elastic critical buckling stress.

7.2 Local Buckling

A method of treatment of partially effective webs during local buckling was developed by LaBoube and Yu (1982) for beams incorporating simple Hat and C sections. The effective widths of the compression flange elements were calculated *apriori* using the full yield stress F_y and the Winter Formula (Equation (3)). The ultimate moment capacity was thereafter calculated using the effective section modulus based on this reduced compression flange width and a modified maximum permissible stress (F_{bw}) that accounted for the reduction in the effectiveness of the web

$$F_{bw} = F_y[1.21 - 0.00013(\frac{d_1}{t})\sqrt{F_y}] \tag{7}$$

where d_1 is the web depth, t the base metal thickness and F_y the yield stress in MPa, or

$$F_{bw} = F_y[1.21 - 0.000337(\frac{d_1}{t})\sqrt{F_y}] \tag{8}$$

where F_y is the yield stress in ksi. Eqn.(7) was based purely on the relationship between test results and the theoretical expression.

This approach has been adopted in the Australian Standard AS1538-1988. The standard requires that the buckling coefficient K be taken as 4.0 and the elastic modulus E as 200000 MPa (29007 ksi) in calculating the local buckling stress. Comparison of experimental ultimate moments for those specimens that displayed purely local buckling prior to failure and ultimate moment estimates based on the standard is presented in Table 5.

Reasonable agreement was achieved with a mean of 0.969 for the ratio $(M_u)_{test}/(M_u)_{comp}$ compared to a mean ratio of 1.002 quoted by LaBoube and Yu (1982) using the same method (see Table 5). The discrepancy may possibly be due to differences in the properties of the section base metal. LaBoube and Yu used strip with a yield stress of up to 371 MPa (53.8 ksi), while that used in the present test programme averaged 653 Mpa (94.7 ksi) and had an elastic modulus of 230000 MPa (33359 ksi). Table 5 shows that the spread of ratios was similar in both series of tests.

8 CONCLUSIONS

Intermediate stiffeners were found to exert a strong influence on the primary mode of buckling in the compression flanges of profiled steel decks loaded in pure flexure. The primary mode of buckling depended on the size of the intermediate stiffener – distortional buckles were associated with small stiffeners and local buckles were associated with large stiffeners. The predictions of the finite strip elastic buckling analysis were found to agree very well with the experimental results. This analysis, when compared to the test results, revealed two important points. Firstly, variations in section geometry from nominal dimensions had to be accounted for (in particular, the central depression of the compression flange). Furthermore, the change-over point of primary buckling mode from distortional to local occurred at a stiffener height of 5.0 mm in both the numerical and experiment results.

The ultimate moment capacity of the decks proved to increase with stiffener size. The increase was such that a considerable improvement in economy could be achieved for a small increase in stiffener size. There was also a greater loss of section stiffness with the onset of local buckling than with distortional buckling.

For the sections which underwent distortional buckling or local then distortional buckling, a simple design approach to compute the ultimate moment based on the yield stress and an effective section modulus which was a function of the distortional buckling stress proved accurate. For sections which underwent local buckling alone the design approach in Australian Standard AS1538-1988 based on the effective flange width and the maximum stress at the flange-web junction (F_{bw}) was 3 percent unconservative but sufficiently reliable for design purposes.

9 ACKNOWLEDGEMENTS

This paper forms part of a programme of research into the stability of steel structures being carried out in the School of Civil and Mining Engineering at the University of Sydney. Tests were performed in the J. W. Roderick Laboratory for Materials and Structures. Technical and material support throughout the experimental programme was generously provided by Lysaght Brownbuilt Industries Pty Ltd through its representative Michael Celeban. Financial support for laboratory and computer equipment was provided by BHP Research – Melbourne Laboratories. Effective thickness investigations were performed at the Electron Microscope Unit, University of Sydney. The first author is supported by a series of scholarships from the Commonwealth Government, The Civil and Mining Engineering Foundation, The University of Sydney, and BHP Research – Melbourne Laboratories.

10 REFERENCES

American Iron and Steel Institute (1989), "Specification for the Design of Cold-formed Steel Structural Members", 1986 edition with 1989 Addendum, AISI, Washington.

Bernard, E. S., Bridge, R. Q. and Hancock, G. J. (1992), " Intermediate Stiffeners in Cold-Formed Profiled Steel Decks. Part 1 – 'V' Shaped Stiffeners", *Research Report R653*, School of Civil and Mining Engineering, University of Sydney, Australia.

Cheung, Y. K., (1976), *Finite Strip Method in Structural Analysis*, Pergamon Press.

Coan, J.M. (1951), "Large-Deflection Theory for Plates with Small Initial Curvature Loaded in Edge Compression", ASME, *Journal of Applied Mechanics*, 18, pp143-151.

Davids, A. J. and Hancock, G. J. (1986), "Compression Tests of Short Welded I-Sections", ASCE, *Journal of Structural Engineering*, 112(5), May 1986, pp960-

976.

Hancock, G. J. (1977), "Local, Distortional and Lateral Buckling of I-beams", Research Report R312, School of Civil and Mining Engineering, University of Sydney.

Hancock, G.J. (1978), "Local, Distortional and Lateral Buckling of I-Beams", *Journal of Structural Division*, ASCE, 104(ST11), pp1787-1798

Hancock, G.J. (1985), "Distortional Buckling of Steel Storage Rack Columns", *Journal of Structural Engineering*, ASCE, 111(12), pp2770-2783.

Key, P.W, Hasan, S.W. and Hancock, G.J. (1988), "Column Behaviour of Cold-Formed Hollow Sections", *Journal of Structural Engineering*, ASCE, 114(2) pp390-407.

Kwon, Y.B. and Hancock, G.J. (1991), "Strength Tests of Cold-formed Channel Sections Undergoing Local and Distortional Buckling", *Research Report R640*, School of Civil and Mining Engineering, University of Sydney, Australia. *also Journal of Structural Engineering*, ASCE, 117(2), July 1992, (accepted for publication).

LaBoube, R. A. and Yu, W-W. (1982), "Bending Strength of Webs of Cold-Formed Steel Beams", *Journal of Structural Division*, ASCE, 108(ST7), pp1589-1604

Lau, S. C. W. and Hancock, G. J. (1988), "Distortional Buckling Tests of Cold-formed Channel Sections", *Ninth International Specialty Conference on Cold-formed Steel Structures*, pp 45-73, St. Louis, Missouri.

Murray, N.W. and Khoo, P.S. (1981), "Some Basic Plastic Mechanisms in the Local Buckling of Thin-Walled Steel Structures", *Int. J. Mech. Sci.*, 23(12), pp703-713.

Rasmussen, K. J. R. and Hancock, G. J. (1987), "Geometric Imperfections in Plated Structures Subject to Interaction Between Buckling Modes", *Research Report R541*, School of Civil and Mining Engineering, University of Sydney, *also* "Geometric Imperfections in Plated Structures Subject to Interaction Between Buckling Modes", *Thin-Walled Structures*, 6(1988), pp433-452

Sridharan, S. (1982), "A Semi-Analytical Method for the Post-Local-Torsional Buckling Analysis of Prismatic Plate Structures", *International Journal for Numerical Methods in Engineering*, 18, pp1685-97.

Standards Association of Australia, AS1397 (1984), *Steel Sheet and Strip – Hot-Dipped Zinc Coated or Aluminium/Zinc Coated*, Standards Association of Australia, N.S.W., Australia.

Standards Association of Australia, AS4100 (1990), *Steel Structures*, Standards Association of Australia, N.S.W., Australia.

Standards Association of Australia, AS1538 (1988), *Cold-Formed Steel Structures*, Standards Association of Australia, N.S.W., Australia.

Venkataramaiah, K. R. and Roorda, J. (1982), "Analysis of Local Plate Buckling Experimental Data", *Sixth International Specialty Conference on Cold-Formed Steel Structures*, St. Louis, Missouri, pp45-74.

11 NOTATION

A	gross section area
A_e	effective section area
b_1	full width of compression flange
b_2	half width of compression flange
b_3	width of tension flange
b_4	width of longitudinal rib cell
d_{cf}	depth of compression flange depression
D	distortional buckling mode or section depth
E	Elastic modulus
F_y	yield stress in design formula
HWL	buckling half-wavelength
L_1, L_2	north and south lever arms
$M_{cr(d)}$	critical buckling moment for distortional mode
$M_{cr(l)}$	critical buckling moment for local mode
M_u	ultimate moment
M_y	moment at first yield
r	inner radius of corner of test section
s	height of intermediate stiffener
t	thickness of base material
λ	half-wavelength
ν	Poisson's ratio
σ_{cr}	buckling stress
σ_{de}	elastic distortional buckling stress
σ_{max}	maximum stress
σ_u	ultimate tensile stress
σ_y	yield stress

Table 1. Experimental Local Critical Buckling Stress Results

Specimen	Pre-load Moment $kN{\cdot}m$	Total Critical Moment Estimates				Ultimate Moment $kN{\cdot}m$
		Method 1 $kN{\cdot}m$	Method 2 $kN{\cdot}m$	Method 3 $kN{\cdot}m$	Mean $kN{\cdot}m$	
ST21A	0.42	1.78	1.78	1.71	1.76	3.39
ST21B	0.21†	1.28	1.37	-	1.32	2.97
ST22A	0.10	0.52	0.53	0.55	0.53	3.56
ST22B	0.21†	0.51*	0.75*	-	0.63	3.16
ST23A	0.10	0.44	0.40	0.31	0.38	2.65
ST23B	0.21†	0.21*	0.21*	-	0.21	2.38
IST43A	0.63	2.83	3.26	-	3.05	3.85
IST44A	0.52	3.09	3.00	2.88	2.99	4.00
IST44B	0.66‡	-♭	-	-	-	3.68
IST45B	0.66‡	2.88	2.84	-	2.86	3.88
IST46A	0.57	3.84	3.91	3.77	3.84	4.59
IST47A	0.74	3.65	3.47	3.75	3.62	4.56
IST47B	0.85	3.81	3.96	-	3.89	4.57
IST48A	0.69	3.93	-	4.19	4.06	5.42
IST48B	0.65	3.83	3.80	-	3.81	4.54
IST410A	0.61	4.33	4.36	5.03	4.57	5.75
IST410B	0.66‡	4.01	4.04	-	4.03	5.14
IST412B	0.66‡	4.56	4.43	-	4.49	5.59

1.0 kNm = 0.73756 kip ft

† mean pre-load moment for non-stiffened specimens

‡ mean pre-load moment for stiffened specimens

∗ poor estimate due to unclear test data

♭ local buckling mode was not measured for this specimen

Table 2. Experimental Distortional Critical Buckling Stress Results

Specimen	Pre-load Moment $kN{\cdot}m$	Total Critical Moment Estimates			
		Method 1 $kN{\cdot}m$	Method 2 $kN{\cdot}m$	Method 3 $kN{\cdot}m$	Mean $kN{\cdot}m$
IST43A	0.63	1.85	1.87	1.63	1.78
IST44A	0.52	2.67	2.42	2.21	2.43
IST44B	0.66‡	2.11	2.22	-	2.17
IST45B	0.66‡	2.27	2.18	-	2.22
IST46A	0.57	3.84	3.91	3.77	3.84
IST47A	0.74	3.24	3.47	3.81	3.51
IST47B	0.85	3.81	3.96	-	3.89
IST48A	0.69	-♭	-	-	-
IST48B	0.65	3.83	3.80	-	3.82
IST410A	0.61	-♭	-	-	-
IST410B	0.66‡	-♭	-	-	-
IST412B	0.66‡	-♭	-	-	-

1.0 kNm = 0.73756 kip ft

‡ mean pre-load moment for stiffened specimens

♭ distortional buckling mode was not measured for this specimen

Table 3. Experimental and Theoretical Buckling Half-wavelengths

Specimen	Experimental		Numerical		Distortional with depressions (mm)
	Local (mm)	Dist. (mm)	Local (mm)	Dist. (mm)	
ST21A	38-39	-	38.5	-	-
ST21B	38-39	-	39	-	-
ST22A	73-74	-	71	-	-
ST22B	73-74	-	71	-	-
ST23A	95-120	-	103	-	-
ST23B	120	-	103	-	-
IST43A	37	120-135	-*	106	60
IST44A	42-47	152-205	39	137	81
IST44B	40-42	95-120	-*	100	63
IST45B	41	130	-*	131	82
IST46A	35	205	31	201	205
IST47A	33-34	173	32	188	173
IST47B	33	185-195	32	190	196
IST48A	29-30	-†	29	242	196
IST48B	30-31	200	31	200	-
IST410A	29.5	-†	28	268	-
IST410B	-♭	-†	29	242	-
IST412B	30	-†	28	263	-
1.0 mm = 0.03937 inch					

† distortional buckling mode was not recorded

∗ no local minimum in numerical analysis

♭ experimental half-wavelength was not measured

Table 4. Ultimate Strength Determination for Specimens Undergoing Distortional Buckling

Specimen	M_u (test) $kN{\cdot}m$	M_y $kN{\cdot}m$	σ_{de} MPa	F_y MPa	$\frac{(M_u)_{test}}{(M_y)}$	$\sqrt{\frac{F_y}{\sigma_{de}}}$
IST43A	3.85	8.92	141	653	0.431	2.15
IST44A	4.00	8.88	190	653	0.450	1.85
IST44B	3.68	8.95	130	653	0.411	2.24
IST45B	3.88	8.90	176	653	0.436	1.93
IST46A	4.59	9.26	282	653	0.496	1.52
IST47A	4.56	9.01	273	653	0.506	1.55
IST47B	4.57	9.06	244	653	0.504	1.64
IST48B	4.54	9.14	296	653	0.497	1.49
1.0 kNm = 0.73756 kip ft; 1.0 MPa = 0.145038 ksi						

Table 5. Design Estimates of Ultimate Moment with Local Buckling

Specimen	M_u (test) $kN{\cdot}m$	M_u (comp) $kN{\cdot}m$	$\frac{(M_u)_{test}}{(M_u)_{comp}}$
ST21A	3.39	3.328	1.019
ST21B	2.97	3.342	0.889
ST22A	3.56	3.456	1.030
ST22B	3.16	3.475	0.909
ST23A	2.65	2.517	1.053
ST23B	2.38	2.535	0.939
IST48A	5.42	5.58	0.971
IST410A	5.72	5.83	0.986
IST410B	5.14	5.49	0.936
IST412B	5.59	5.82	0.960
Mean			0.969
Standard Deviation			0.053
1.0 kNm = 0.73756 kip ft			

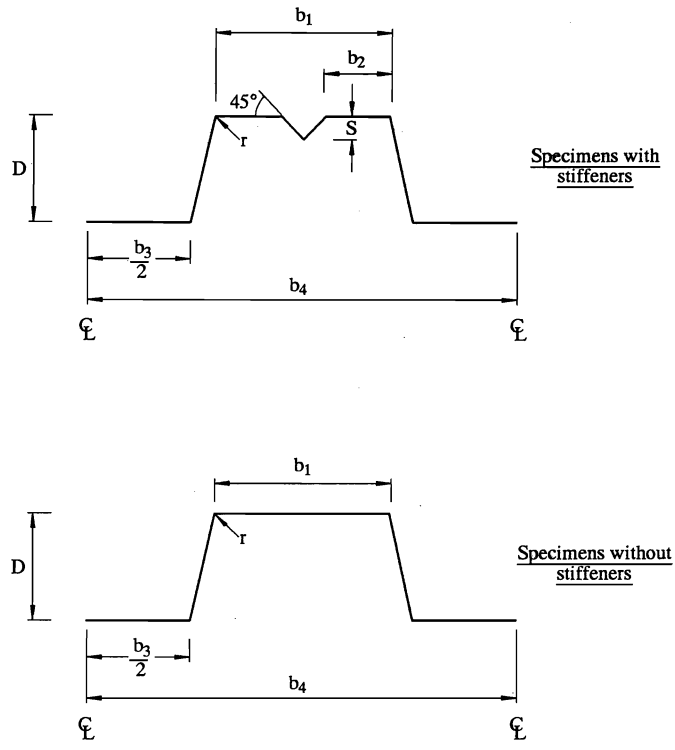

Figure 1. Geometry of Sections

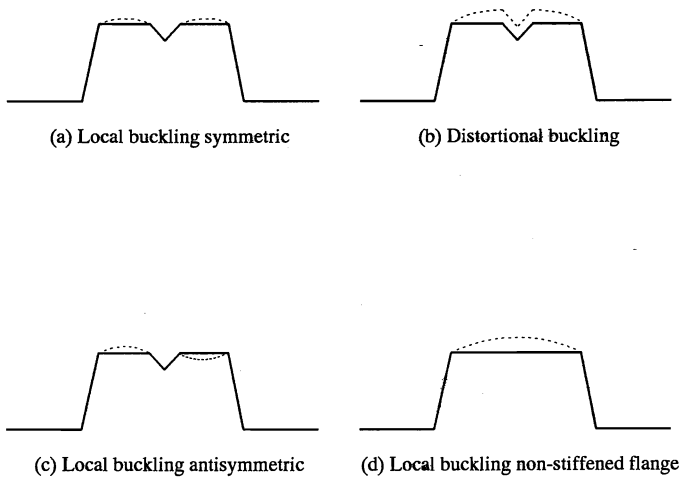

Figure 2. Buckling Modes Encountered in Tests

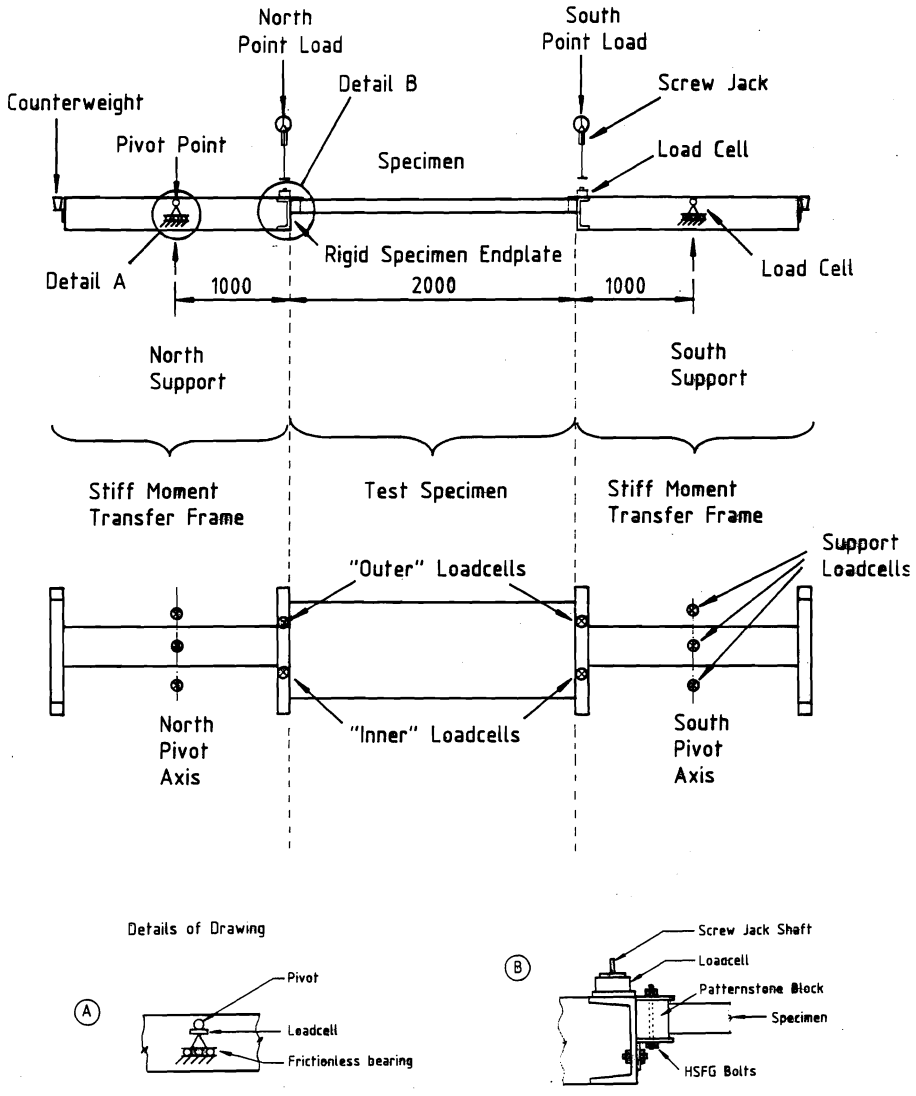

Figure 3. Elevation and Plan of Test Apparatus

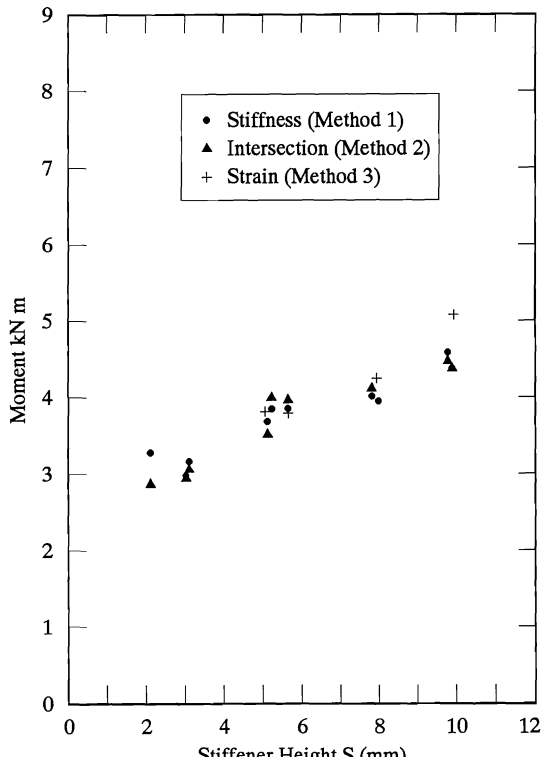

a) Experimental Raw Data

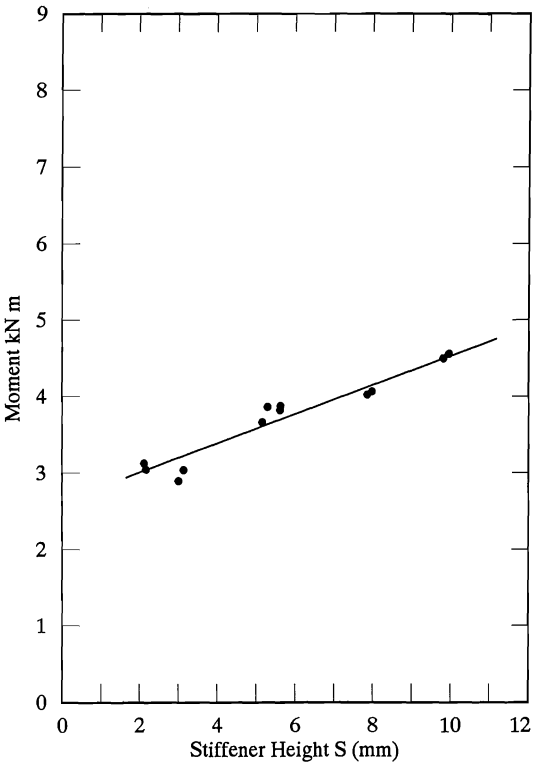

b) Mean Experimental Buckling Moments

Figure 4. Local Buckling Moment Results

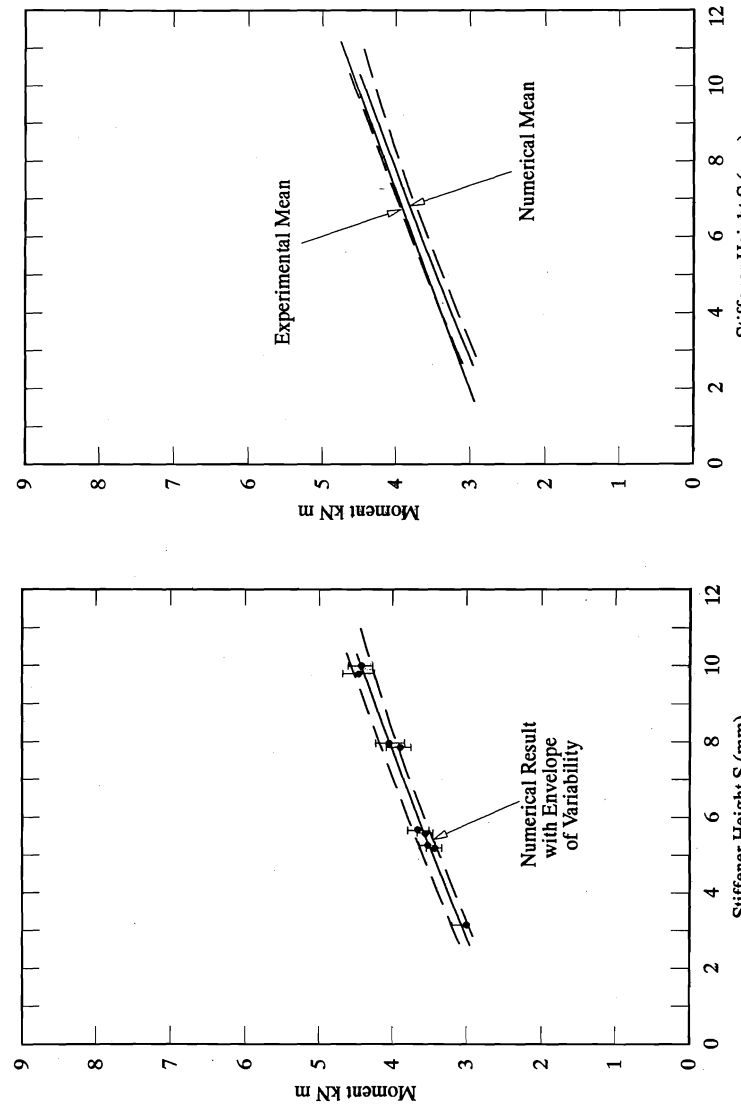

c) Numerical Estimates and Envelope of Variability

d) Comparison of Experimental Results and Envelope of Variability

Figure 4. Local Buckling Moment Results (cont.)

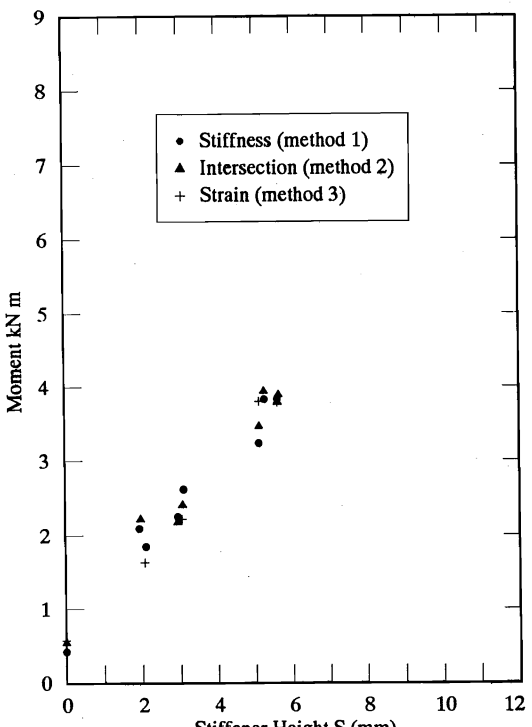

a) Experimental Raw Data

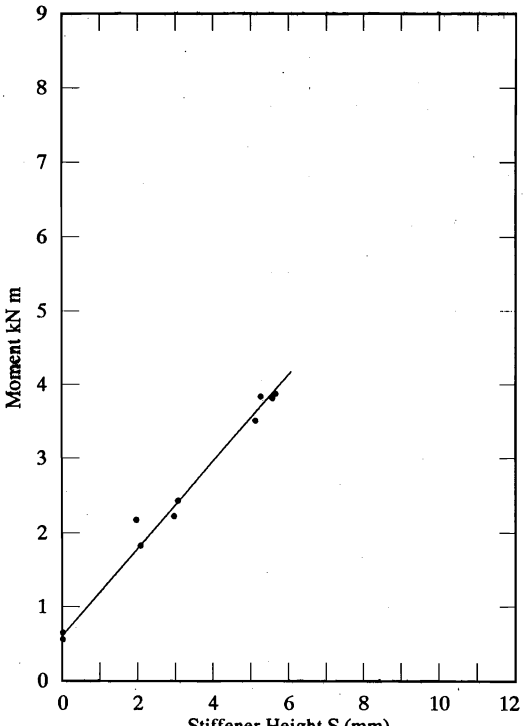

b) Mean Experimental Buckling Moments

Figure 5. Distortional Buckling Moment Results

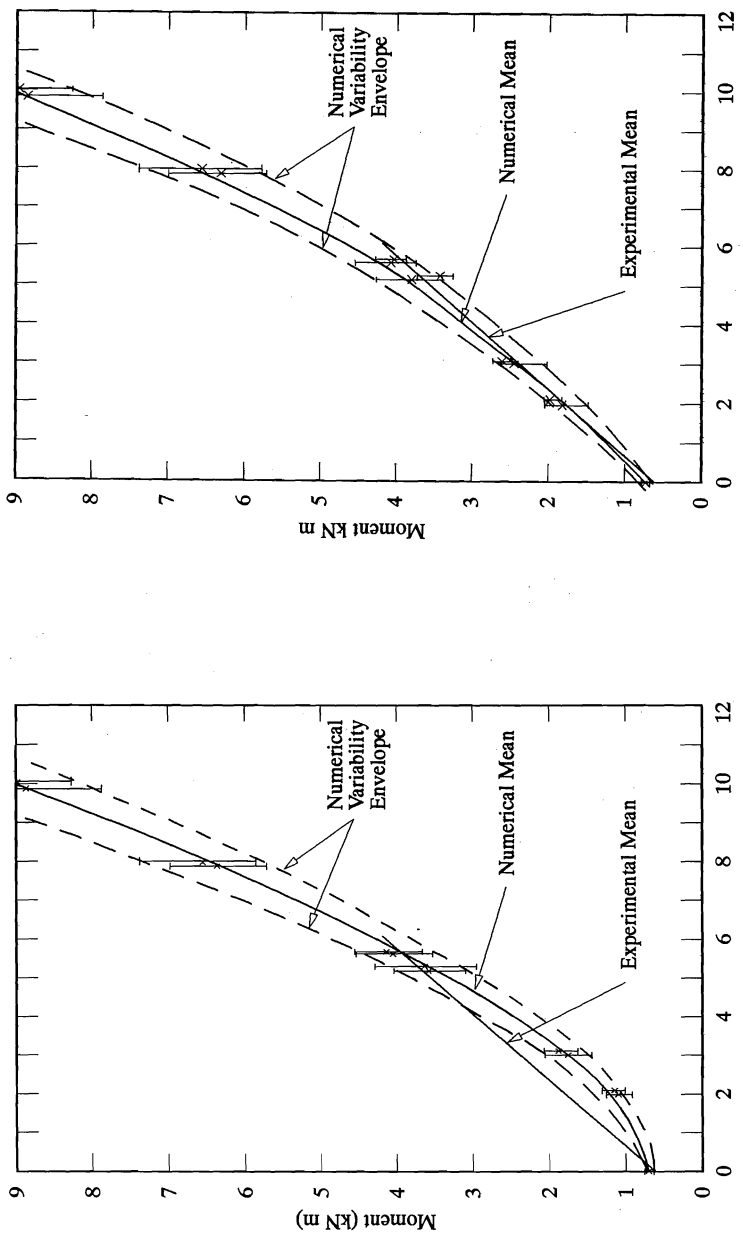

c) Numerical Estimates and Envelope of Variability for Geometry Without Flange Depression

d) Numerical Estimates and Envelope of Variability for Geometry With Flange Depression

Figure 5. Distortional Buckling Moment Results (cont.)

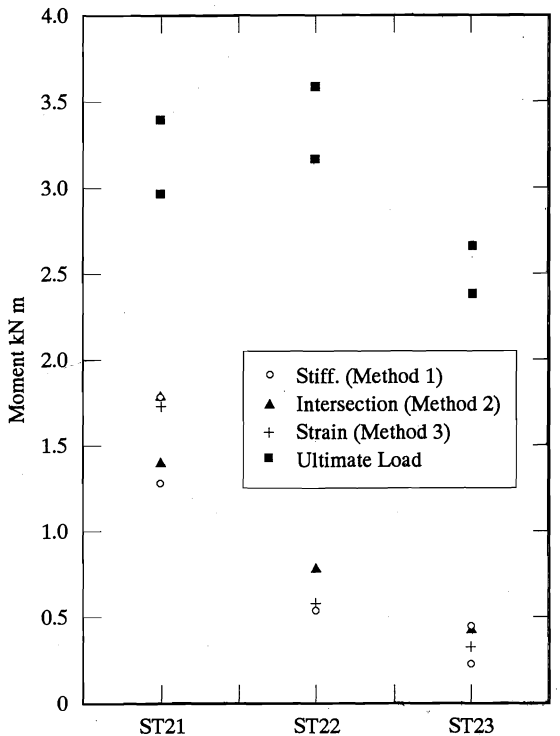

a) Experimental Raw Data and Ultimate Moments

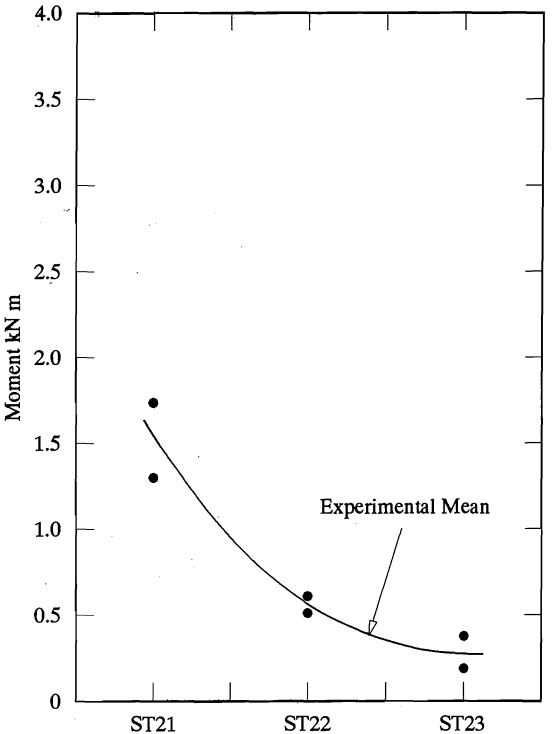

b) Mean Experimental Buckling Moments

Figure 6. Local Buckling Moments for Sections Without Intermediate Stiffeners

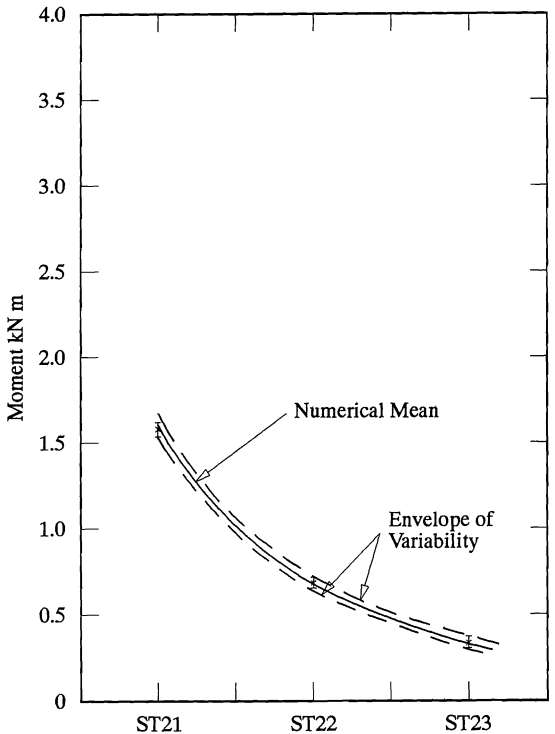

c) Numerical Estimates and Envelope of Variability

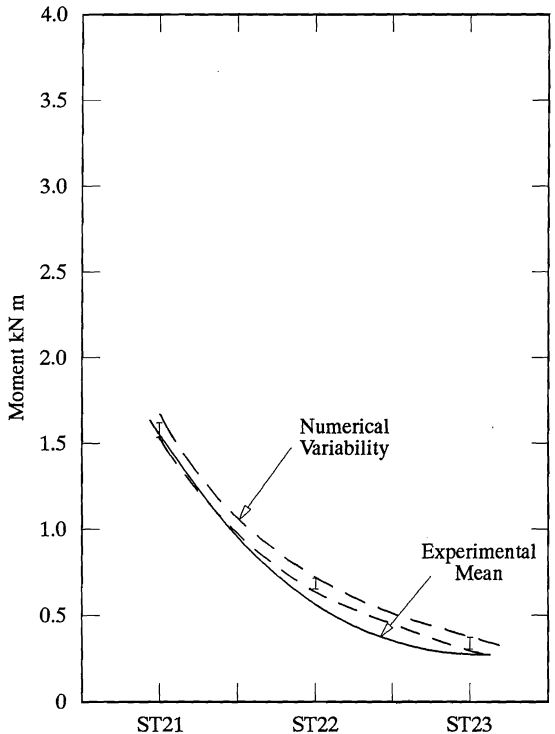

d) Comparison of Experimental Results and Envelope of Variability

Figure 6. Local Buckling Moments for Sections Without Intermediate Stiffeners (cont.)

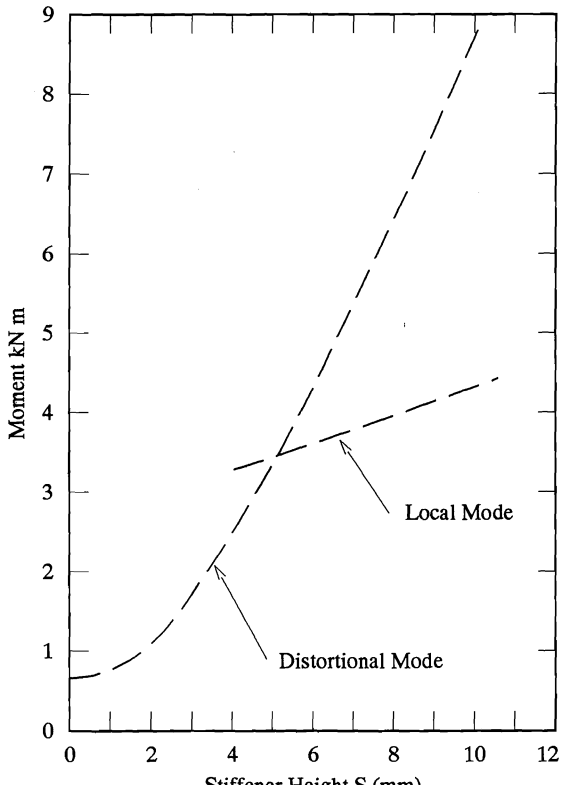

Fig. 7 Local and Distortional Buckling Results for Ideal Geometry

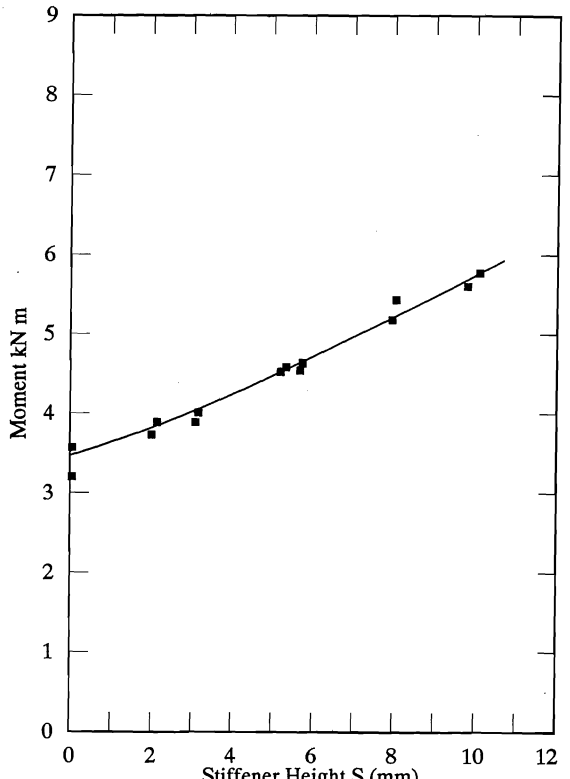

Fig. 8 Ultimate Moments for Sections with Intermediate Stiffeners

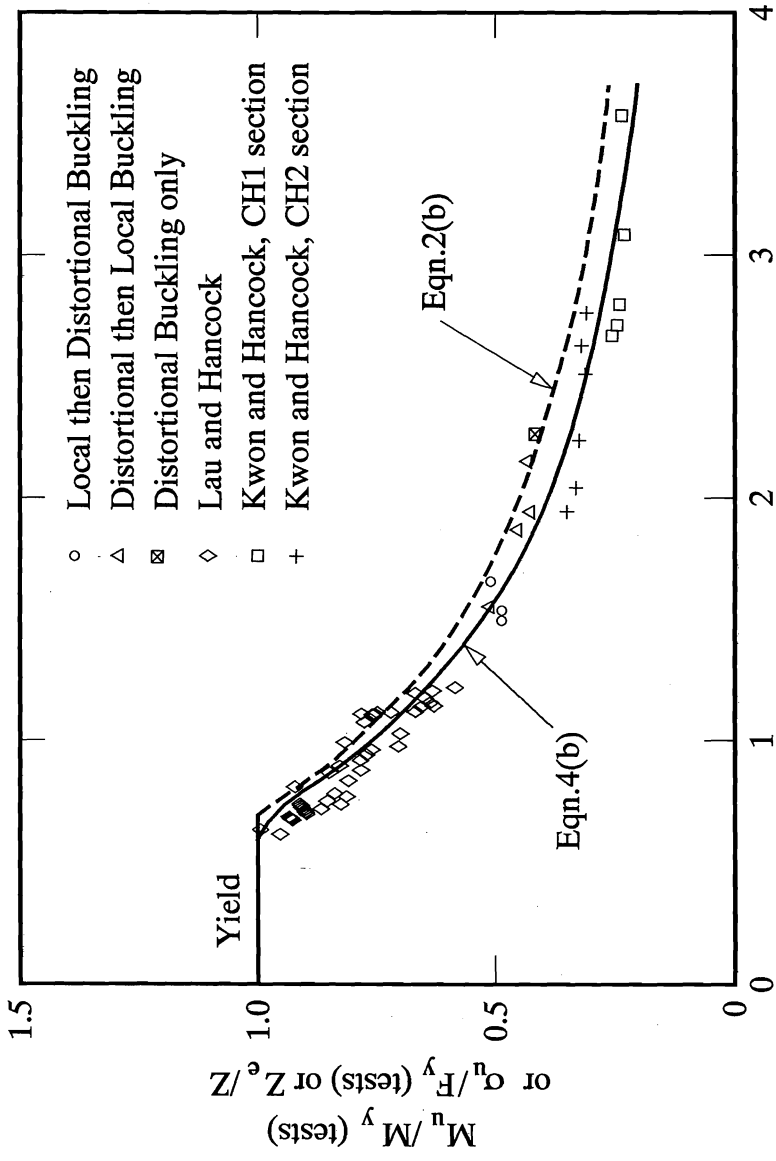

Fig. 9 Comparison of Test Results and Design Curves.